

1 Observed global ocean phytoplankton phenology indices.

2 Sarah-Anne Nicholson¹, Thomas J. Ryan-Keogh¹, Sandy J. Thomalla^{1,2}, Nicolette Chang^{1,5},
3 Marié E. Smith^{3,4}

4 ¹Southern Ocean Carbon-Climate Observatory, CSIR, Cape Town, South Africa

5 ²Marine and Antarctic Research Centre for Innovation and Sustainability, University of Cape Town, Cape Town,
6 South Africa

7 ³Coastal Systems and Earth Observation Research Group, CSIR, Cape Town, South Africa

8 ⁴Department of Oceanography, University of Cape Town, Cape Town, South Africa

9 ⁵Global Change Institute, University of the Witwatersrand, Johannesburg, South Africa

11 *Correspondence to:* Sarah-Anne Nicholson (snicholson@csir.co.za)

12

13 Abstract

14 Phytoplankton bloom phenology is an important indicator for the monitoring and management of marine resources
15 and the assessment of climate change impacts on ocean ecosystems. Despite its relevance, there is no long-term
16 and sustained observational phytoplankton phenological product available for global ocean implementation. ~~This~~
17 ~~need is addressed~~ here ~~by providing a~~ phenological ~~data product~~ (including among other seasonal metrics, the
18 bloom initiation, termination, duration, and amplitude timing) using satellite derived chlorophyll-a data from the
19 Ocean Colour Climate Change Initiative. This ~~multi-decadal data~~ product provides the phenology output from
20 three widely used bloom detection ~~methods~~ at three different spatial resolutions (4, 9 and 25 km) allowing for
21 both regional and global-scale applications. ~~When compared to each other on global scales, there is a general~~
22 agreement between the detection methods and between ~~the~~ different resolutions. Regional differences are evident
23 in coastal domains (particularly for ~~different resolutions~~) and in regions with strong transitions (~~notably for~~
24 ~~different detection methods~~). This product can be used towards the development of national and global
25 biodiversity assessments, pelagic ecosystem mapping and for monitoring change in climate sensitive regions
26 relevant for ecosystem services. The dataset is published in the Zenodo repository under the following DOIs, 4
27 km: ~~https://doi.org/10.5281/zenodo.8402932~~, 9 km: ~~https://doi.org/10.5281/zenodo.8402847~~ and 25 km:
28 ~~https://doi.org/10.5281/zenodo.8402823~~ (Nicholson et al., 2023a, b, c) and will be updated ~~on annual basis~~.

Deleted: The data product presented

Deleted: addresses this need through the development of

Deleted: detection algorithms

Deleted: algorithms

Deleted: In this study, the mean global phenology is characterised according to the three phenological detection methods and the different resolutions, which are

Deleted: one another. In general

Deleted: good

Deleted: on global scales

Deleted: resolution

Deleted: between phytoplankton seasonal characteristics.

Deleted: ~~https://doi.org/10.5281/zenodo.8402932~~, 9 km: ~~https://doi.org/10.5281/zenodo.8402847~~

Deleted: ~~https://doi.org/10.5281/zenodo.8402823~~

Deleted: regularly

1 Introduction

The seasonal proliferation of phytoplankton across the world's ocean is a ubiquitous signal visible from space, and one that plays a crucial role in the Earth system. Phytoplankton "blooms" capture 30-50 billion metric tons of carbon annually, representing almost half of the total carbon uptake by all plant matter (Buitenhuis et al., 2013; Carr et al., 2006; Falkowski, 1994; Field et al., 1998; Longhurst et al., 1995). Their key role in driving the strength and efficiency of the biological carbon pump, the transfer of atmospheric carbon to the deep ocean interior, is a crucial component of the global carbon cycle and instrumental in the assessment of climate feedbacks and change (DeVries, 2022; Henson et al., 2011). Phytoplankton also mediate climate through the production of important atmospheric trace gases such as nitrous oxide, a potent greenhouse gas, and volatile organic carbons such as dimethyl sulphide, that have a significant impact on cloud formation and global albedo (Charlson et al., 1987; Korhonen et al., 2008; McCoy et al., 2015; Park et al., 2021). As the foundation of the marine food chain, phytoplankton are critical to supporting higher trophic levels and a lucrative fisheries industry that impacts global food security (Gittings et al., 2021; Stock et al., 2017). There is an enormous benefit to society in being able to predict ecosystem responses to environmental change, by providing the knowledge necessary for competent decision-making. As such understanding, characterising and accurately predicting changes in the annual cycle of phytoplankton blooms provides an essential tool for managing marine resources and for predicting future climate change impacts (Thomalla et al., 2023; Tweddle et al., 2018).

Phytoplankton phenology refers to the timing of seasonal activities of phytoplankton biomass and is used widely as an indicator to characterise phytoplankton blooms and to monitor their variability over time. Adjustments in the characteristics of phenology typically reflect alterations in ecosystem function that may be linked to environmental pressures such as climate change (Henson et al., 2018; Racault et al., 2012; Thomalla et al., 2023). Key phenological phases of phytoplankton bloom development include: the time of initiation, the time of maximum concentration (amplitude), the time of termination and duration as the time between initiation and termination. These phytoplankton bloom phases are typically driven by seasonal changes in physical forcing (such as incoming solar radiation, water column mixing and nutrient depletion), which are generally linked to large-scale climate drivers (Racault et al., 2012; Thomalla et al., 2023). The timing of the bloom initiation and amplitude is particularly critical for efficient trophic energy transfer, which can be impacted negatively through trophic decoupling. For example, mismatches between bloom timing and zooplankton grazing can lead to suboptimal food conditions for higher trophic levels which in turn has been linked to the collapse of crucial fisheries (Cushing, 1990; Koeller et al., 2009; Seyboth et al., 2016; Stock et al., 2017). Bloom duration impacts the amount of biomass being generated within a season that can be exported to the ocean's interior or transferred to higher trophic levels via the marine food web and can thus play a more important role than bloom magnitude (Barnes, 2018; Rogers et al., 2019). Bloom timing has also been shown to influence the seasonal cycles of CO₂ uptake, primary production and the efficiency of carbon export and storage (Bennington et al., 2009; Boot et al., 2023; Lutz et al., 2007; Palevsky and Quay, 2017). Having access to a global data product that characterises the seasonal cycle of phytoplankton over the last 25 years and into the future can thus provide a valuable tool to users that require an understanding of key aspects of the growing season and how these may be changing over time.

Deleted: monitor

Formatted: Font colour: Custom Colour (RGB(28,29,30)), Highlight

Current generation Earth System Models (ESMs) show that phytoplankton phenology is changing and will continue to change in response to a warming and more stratified ocean (Henson et al., 2018; Yamaguchi et al., 2022). For example, blooms are predicted to initiate later in the mid-latitudes and earlier at high and low latitudes by ~5 days per decade by the end of the century (Henson et al., 2018). But what about changes in bloom phenology in the contemporary period? Satellite-based ocean colour remote sensing, which provides estimates of chlorophyll-a (chl-a) concentrations (a proxy for phytoplankton abundance), is the only observational capability that can provide synoptic views of upper ocean phytoplankton characteristics at high spatial and temporal resolution (~1 km, ~daily) and high temporal extent (global scales, for years to decades). In many cases, these are the only systematic observations available for chronically under-sampled marine systems such as the polar oceans. In 1997, the first global ocean colour observing satellite (SeaWiFS) was launched and these observations have been sustained through a successive series of additional ocean colour satellites (MODIS, MERIS, VIIRS, OLCI). These have all been merged by the European Space Agency into the Ocean Colour Climate Change Initiative (OC-CCI) remotely-sensed observational data product, which provides ~25 years of ocean colour data for climate change assessment (Sathyendranath et al., 2019). We note however that despite their obvious spatial and temporal advantages, remotely detected water-leaving radiances emanate from only the first optical depth, and give little quantitative information about the vertical structure of the water column, which can be particularly important in low nutrient regions where a subsurface chl-a maxima is prevalent. In addition, we recognise that the OC-CCI chl-a observational data product may exhibit regional biases (that can vary in both magnitude and direction) and arise from several factors inherent to both satellite remote sensing technology and the complexities of ocean ecosystems. One example is that algorithms are often regionally trained on datasets from specific parts of the world, which can result in discrepancies when applied globally. Despite these regional biases, satellite ocean colour chl-a observational data products remain highly valuable, especially when the goal is to identify patterns in the seasonal cycle of phytoplankton and how these patterns evolve over time. While local accuracy may be impacted by biases, the broader trends—such as the timing of spring blooms, the intensity of summer productivity, or the length of growing season—are still well captured. This is because biases tend to be relatively consistent over time in any given region, allowing researchers to focus on changes in these patterns rather than on the absolute values. These long-term changes in the seasonal cycle are crucial for understanding how marine ecosystems respond to environmental stressors like warming temperatures, ocean acidification, and changes in nutrient availability.

The estimation of phytoplankton phenology from OC-CCI remote sensing of chl-a can provide important information of the rates of change in key indices on a global scale for comparison to those derived from ESM's. For example, a recent study by Thomalla et al., (2023) determined the trends in phenology metrics in the Southern Ocean using 25 years of satellite-derived chl-a (1997-2022) data. Their results revealed that large regions of the Southern Ocean expressed significant trends in phenological indices that were typically much larger (e.g. <50 days decade⁻¹) than those reported in previous climate modelling studies (< 5-10 days decade⁻¹), which suggests that ESM's may be underestimating ongoing environmental change. Thomalla et al., (2023) conclude, that seasonal adjustments of this magnitude at the base of the food web may impact the nutritional stress, reproductive success, and survival rates of larger marine species (e.g., seals, seabirds, and humpback whales), in particular if they are unable to synchronise their feeding and breeding patterns with that of their food supplies. It is anticipated

Deleted: ¶

Deleted: this data product on a global scale

Deleted:), (Thomalla et al., 2023) recently

Deleted:).

Deleted: A

129 ~~that a~~ similar analysis using these key phytoplankton metrics applied to the global ocean ~~or specific regions of~~
 130 ~~interest~~ will reveal regional sensitivities of ecosystems to change with important implications for ecosystem
 131 function and ~~associated societal impacts~~. There is also a need for the continuous monitoring and ~~ongoing~~
 132 assessment of the seasonal adjustments of phytoplankton on global scales (in addition to continued benchmarking
 133 for ESMS), ~~which would require regular updates of key phenological metrics going forward. Such information is~~
 134 relevant for effective marine management programs and early detection of vulnerabilities in key regions, e.g.,
 135 those necessary for sustaining fisheries. In addition, a phenology data product such as this can provide a useful
 136 aid for the planning of oceanographic research campaigns ~~that wish to align with or determine their occupation~~
 137 ~~relative to key aspects of the growing season. Finally, this data product could also be valuable to support those~~
 138 ~~users without the programming know-how or access to computationally expensive resources that are required to~~
 139 ~~generate it.~~

141 ~~Here~~ we present a new global phytoplankton phenological ~~data product with indicators that include~~ among other
 142 metrics bloom initiation, termination, amplitude, and duration. ~~These metrics are~~ computed using three different
 143 gridded resolutions (4, 9 and 25 km) and with three different methodologies of determining ~~phenology. This~~
 144 ~~derived observational data product facilitates the global characterisation of the climatological seasonal cycle and~~
 145 ~~can be used to identify the sensitivity of the seasonal cycle to change (through the analysis of trends and~~
 146 ~~anomalies). The phenology~~ data product is currently available from 1997 until 2022 and will be updated annually
 147 and in sync with any version updates of the OC-CCI chl-a ~~observational~~ data product.

148 2 Methodology

149 2.1 Data and pre-processing

150 Satellite-derived chl-a concentrations (mg m^{-3}) were obtained from the European Space Agency (ESA), from OC-
 151 CCI (<https://esa-oceancolour-cci.org>; (Sathyendranath et al., 2019) at 4 km and 8-day resolution. The latest
 152 available OC-CCI product (version v6.0, released on 04/11/2022) is used in this present study. This version marks
 153 a substantial change to previous versions (e.g., v5.0, see Sathyendranath et al., (2021)) in that it incorporates
 154 Sentinel 3B OLCI data, the MERIS-4th reprocessing dataset, upgraded Quasi-Analytical algorithm (QAAv6) and
 155 the exclusion of MODIS and VIIRS data after 2019 (refer to D4.2 - Product User Guide for v6.0 Dataset from
 156 <https://climate.esa.int/en/projects/ocean-colour/key-documents/> ~~for further details on processing and validation~~).
 157 ~~The OC-CCI observational data product was generated with the specific aim of studying phytoplankton dynamics~~
 158 ~~at seasonal to interannual scales. Indeed, it has been used widely by the scientific community for studying~~
 159 ~~phytoplankton phenology (e.g., Anjaneyan et al., 2023; Delgado et al., 2023; Ferreira et al., 2021; Gittings et al.,~~
 160 ~~2019, 2021; Racault et al., 2017; Silva et al., 2021; Thomalla et al., 2015, 2023).~~ Data provided by OC-CCI
 161 covered the period from 29/08/1997 – 27/12/2022 for the global ocean (90°N – 90°S and 180°E – 180°W).

163 The phenological indices described below are calculated using three horizontal resolutions in surface chl-a, the
 164 native 4 km resolution as provided by OC-CCI and a regridded 9 km and 25 km horizontal resolution. The 4 km

Deleted: climate.

Deleted: to have a global phytoplankton phenology product such as this annually updated to allow

Deleted:). These assessments of the sensitivity of key ecosystems to change are

Deleted: among many other applications

Formatted: Font colour: Auto, Not Highlight

Deleted: In this paper,

Deleted: data product consisting of

Deleted: (including

Deleted:)

Deleted: key metrics. The

Deleted: ,

Deleted: <https://climate.esa.int/en/projects/ocean-colour/key-documents/>).

Formatted: Font colour: Blue

179 and 9 km resolutions are considered important for smaller-scale regional needs such as coastal applications and
180 field campaigns. The 25 km resolution is the most computationally efficient for users to work with, it results in a
181 reduction of missing data and is useful for global open-ocean applications. For the 9 km and 25 km resolutions,
182 chl-a is regridded onto a regular grid through bilinear interpolation using the xESMF Python package (Zhuang et
183 al., 2023). In all resolutions for phenological detection, data gaps were reduced further by applying a linear
184 interpolation scheme in sequential steps of longitude, latitude, and time (Racault et al., 2014). A two-point limit
185 (e.g., the maximum number of consecutive empty grid cells to fill) is chosen for the interpolation to avoid
186 overfilling of regions that contain larger coherent data gaps. We further apply a 3 time-step (24 days) rolling mean
187 along the time dimension to avoid any outliers that may result in fake detection points. However, for the Seasonal
188 Cycle Reproducibility (SCR) computations only interpolation (time, lat and lon) is carried out, this is discussed
189 further below.

190 2.2 Phenological Indices and Detection

191 Phytoplankton blooms typically manifest as a seasonal cycle, with a bloom initiation that identifies the timing of
192 the ramp up in phytoplankton growth and biomass accumulation followed by bloom peaks within the growing
193 season (which could be multiple) and finally the bloom termination, which defines the end of the growing season.
194 The phenological indices applied here are based on those applied to the SO in Thomalla et al. (2023). To calculate
195 the phenological indices for initiation and termination, we apply three main detection methods used by the
196 community (e.g. Brody et al., 2013; Ji et al., 2010), which are detailed below (iii and iv). Each detection method
197 has its strengths and weaknesses, and therefore the choice of method for application can be determined by the user
198 needs, which are elaborated on in Brody et al. (2013). These methods were chosen over other approaches (e.g.
199 Platt et al., 2009; Rolinski et al., 2007) due to the method's suitability for estimates across global scales as it is
200 capable of encompassing a wide range of different shapes in phytoplankton blooms (Racault et al., 2012). In this
201 **derived observational** data product, all three approaches are provided globally at all three resolutions. Below we
202 outline the series of steps implemented for estimating the global phenological indices and provide an
203 accompanying flow chart (Figure 1) to illustrate the succession of steps being implemented. In addition, we
204 provide some example applications at four key observing stations (Figure A1) to facilitate a visualisation of the
205 derived phenological indices from four annual time series.

206
207 (i) Bloom maximum climatology: The climatological peak (maximum amplitude) of the bloom was identified as
208 the local maximum in chl-a occurring within each grid cell's 25-year climatology. This approach was necessary
209 because the timing of bloom events varies globally, i.e., southern hemisphere blooms typically occur during austral
210 spring - summer (September - February), while northern hemisphere blooms occur in boreal spring - summer
211 (April - August) (Racault et al., 2012). Furthermore, both hemisphere tropics tend to be approximately 6 months
212 out of phase with both hemisphere higher latitude regions. As such, it would be inappropriate to use a fixed date
213 period (or "bloom slice" see below) to identify bloom occurrence on global scales. Instead, for each grid cell we
214 calculate the 8-day mean climatology. The date of the maximum climatological bloom for each pixel is then used
215 to centre the timing of the phenology detection **methods** described below.

Deleted: (

Deleted: .,

Deleted:).

Deleted: (

Deleted: .,

Deleted:).

Deleted:).

Deleted:).

Deleted: algorithms

(ii) Identification of bloom peaks: For every pixel on a year-by-year basis we take the climatological bloom maximum peak ± 6 months and determine the date and magnitude of the bloom maximum peak for each year. To ensure that seasonal blooms with more than one peak could be accounted for, multiple bloom peaks were defined as a second, third, or n^{th} local maxima where the chl-a concentration reached at least 75% of the amplitude of the bloom maximum peak magnitude and were a minimum of 24 days (i.e., 3 x 8 day time intervals) away from the bloom maximum peak for that year. The 75% threshold was chosen to identify peaks with similar magnitude to the bloom maximum peak so as to allow for the occurrence of a multiple peak growing season. Choosing a threshold higher than this would likely exclude recognisable bloom peaks (which could lead to an underestimate of the bloom duration), while choosing a lower threshold may include sub-seasonal variability and lead to an overestimation of the bloom duration. These additional peaks were found within ± 6 months of the maximum peak. An example of such a multi-peak bloom detection is provided in Figure 1 and Figure A1c. The additional peaks were identified with the Python SciPy (Virtanen et al., 2020) function ‘find_peaks’.

(iii) The ‘bloom slice’: The bloom slice, used to find the bloom initiation and termination dates, is identified for each pixel as the 6-month time span preceding and following from the maximum bloom peak (ii). Or in the case of multi-modal blooms, 6-months preceding the first and following the last peak respectively.

(iv) Bloom initiation: The bloom initiation date for each bloom slice as described in (iii) is calculated as the first date before either the bloom maximum, or the first peak in the event of multi-modal blooms, according to the following thresholds:

1. *Biomass-based threshold method (TS)*: First determine the range as the difference in chl-a concentration between the bloom maximum and preceding minimum. Then identify the bloom initiation as the first date that the chl-a concentration was greater than the minimum chl-a concentration plus 5% of the chl-a range.
2. *Cumulative biomass-based threshold method (CS)*: First remove any values preceding the bloom slice minimum chl-a concentration and any values greater than 3 times the median of the bloom slice, before calculating the cumulative sum of chl-a. Then identify the first date that the chl-a concentration was greater than 15% of the total cumulative chl-a concentration.
3. *The rate of change method (RC)*: First determine the rate of change of the bloom slice and then identify the first date that the chl-a rate of change was greater than 15% of the median rate of change in chl-a concentration.

To note, the choice of above chosen percentage thresholds are in accordance with those used by previous phenological detection studies (Brody et al., 2013; Henson et al., 2018; Hopkins et al., 2015; Ji et al., 2010; Thomalla et al., 2011, 2015, 2023).

(v) Bloom termination: The bloom termination date for each bloom slice was similarly calculated as the first date after the bloom maximum, or the last peak in the event of multi-modal blooms, according to the following thresholds:

1. *TS*: the first date that the chl-a concentration was less than the minimum chl-a concentration plus 5% of the chl-a range.

Deleted:

Formatted: Outline numbered + Level: 1 + Numbering Style: 1, 2, 3, ... + Start at: 1 + Alignment: Left + Aligned at: 0,63 cm + Indent at: 1,27 cm

Deleted: ¶

Formatted: Outline numbered + Level: 1 + Numbering Style: 1, 2, 3, ... + Start at: 1 + Alignment: Left + Aligned at: 0,63 cm + Indent at: 1,27 cm

267 2. CS: the first date that the chl-a concentration was less than 15% of the total cumulative chl-a
268 concentration.

269 RC: the first date that chl-a rate of change was less than 15% of the median rate of change in chl-a
270 concentration. (vi) Bloom duration: The bloom duration was calculated as the number of days between the bloom
271 initiation and termination dates. This is applied to each phenological detection method described above (TS, CS
272 and RC).

273
274 (vii) Integrated and mean bloom chl-a: The seasonally integrated bloom chl-a was calculated using the NumPy
275 (Harris et al., 2020) trapezoidal function as the chl-a concentration integrated between the bloom initiation and
276 termination dates. The seasonal mean chl-a was calculated as the average chl-a between the bloom initiation and
277 termination dates. These are applied to each of the three phenological detection methods described above (TS, CS
278 and RC).

279
280 (viii) SCR: The variance of the seasonal cycle was calculated as defined in Thomalla et al., (2023), where the SCR
281 is the Pearson's correlation coefficient of the annual seasonal cycle correlated against the climatological mean
282 seasonal cycle. A value of 100% is indicative of an annual seasonal cycle that is a perfect repetition of the
283 climatological mean, while a value of 0% means that there is no annually reproducible mean seasonal cycle.
284 Unlike for phenological indices i-vii, for SCR the original OC-CCI v6.0 data were used for the three different grid
285 resolutions, however with only spatial-temporal interpolation for gap filling and no rolling mean to avoid
286 smoothing out temporal variability. For SCR for each pixel the bloom slice is restricted to 12 months (i.e., January
287 to December).

288
289 The cyclical nature of the year day calendar presents a significant challenge when calculating means and standard
290 deviations of phenological indices. For example, we need to avoid a situation where the mean bloom initiation
291 between a year with a bloom in December (day of year = 340) and a year with a bloom in January (day of year =
292 10) is incorrectly calculated as an average bloom initiation date in July (day of year = 175). To address this, as
293 similarly applied in Thomalla et al. 2023, we used the Python SciPy function circmean (or circstd for standard
294 deviation), which calculates circular means for samples within a specified range, correctly identifying the mean
295 as day of year 357.

296

Deleted: .
(

Deleted:),

Deleted: To generate climatological means we used the Python SciPy function 'circmean' which calculates circular means for samples in a range.

Formatted: Font colour: Black, Highlight

Deleted: e.g.,

Deleted: 350

Deleted: e.g.,

Formatted: Font colour: Black, Highlight

Formatted: Font colour: Black, Highlight

Formatted: Font colour: Black, Highlight

Deleted: 20

Deleted: e.g.,

Deleted: 185), where

Formatted: Font colour: Black, Highlight

Formatted: Font colour: Black, Highlight

Deleted: correct

Formatted: Font colour: Black, Highlight

Formatted: Font colour: Black, Highlight

Deleted: is in January (e.g.,

Deleted: 3).

Formatted: Font colour: Black, Highlight

Formatted: Font colour: Black

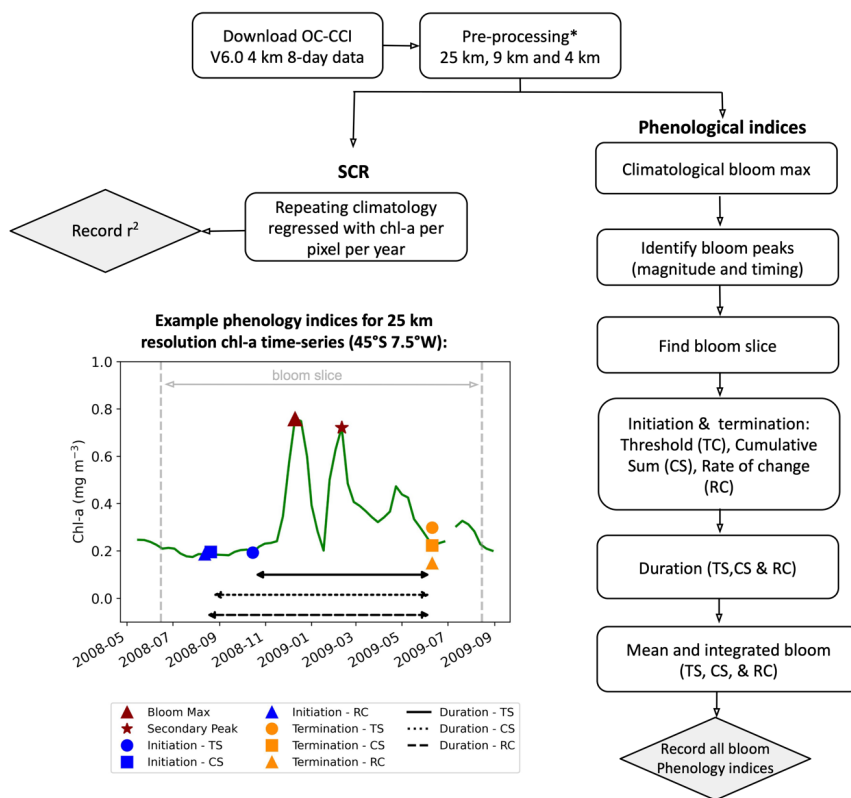


Figure 1: Methodological flow chart outlining the steps taken to calculate the phytoplankton seasonal metrics. An example time-series illustrating the performance of the resulting phenological indices for a bimodal (double peak) bloom in the Southern Ocean (45°S, 7.5°W) is provided for the three different phenological methods, biomass-based threshold (TS), cumulative sum (CS) and rate of change (RC). *See Methodology for pre-processing steps.

3 Results and Discussion

3.1 Global open-ocean phytoplankton seasonal metrics

A significant degree of regional variability is evident in the mean distribution of seasonal metrics (bloom amplitude, timing, and seasonality) (Figure 2). Bloom magnitude metrics (max bloom chl-a, mean bloom chl-a and integrated bloom chl-a; Figure 2a-c) are all higher in the high-latitudes and in the coastal regions, particularly in the Eastern Boundary Current Systems, and lowest in the oligotrophic subtropical gyres. There is a general

325 equator-to-pole symmetry in the timing of phytoplankton blooms between the northern and southern hemispheres.
326 In the subpolar regions phytoplankton blooms initiate in the northern hemisphere during Boreal Spring to early
327 summer (March-May) and in the southern hemisphere in Austral Spring to early summer (September-November)
328 in response to light availability (Sverdrup, 1953) (Figure 2d). While in the subtropics, where there is ample light
329 throughout the year, blooms typically initiate in autumn to winter in response to nutrient supplies through winter-
330 driven deepening of the mixed-layer (Fauchereau et al., 2011; Thomalla et al., 2011). In both the Antarctic and
331 Arctic polar regions, phytoplankton blooms initiate in Austral (December) and Boreal summer (July), when the
332 sea-ice cover melts. The timing of bloom maximum follows the same equator-to-pole symmetry as bloom
333 initiation (Figure 2g), with high latitude regions peaking in Austral and Boreal summer, whereas the subtropics
334 peak in Austral and Boreal winter. This large-scale meridional structuring of the bloom timing is as expected and
335 similarly found in previous large-scale satellite based phenological studies (Kahru et al., 2011; Racault et al.,
336 2012; Sapiano et al., 2012). There is a larger degree of spatial heterogeneity in bloom termination (Figure 2e),
337 particularly evident in regions such as the high latitude North Atlantic and sub-Antarctic, with terminations that
338 extend up to 6 months later in comparison to surrounding areas which were initiated at a similar time. This
339 manifests in zonal asymmetries across the different basins for bloom duration (Figure 2f), with considerably
340 longer blooms occurring in the Pacific basin compared with the Atlantic and Indian basins. SCR covers a large
341 range of variability across latitudinal bands. Notably, SCR (Figure 2h) is oftentimes low in regions where bloom
342 duration is long, and this relationship is strongest in the tropical Pacific ($r \sim -0.4$). In the Southern Ocean, long-
343 sustained but highly variable blooms were proposed as a response to intermittent physical forcing (high-frequency
344 wind and meso to submesoscale dynamics) that entrain nutrients and postpone the seasonal termination (Thomalla
345 et al., 2011).

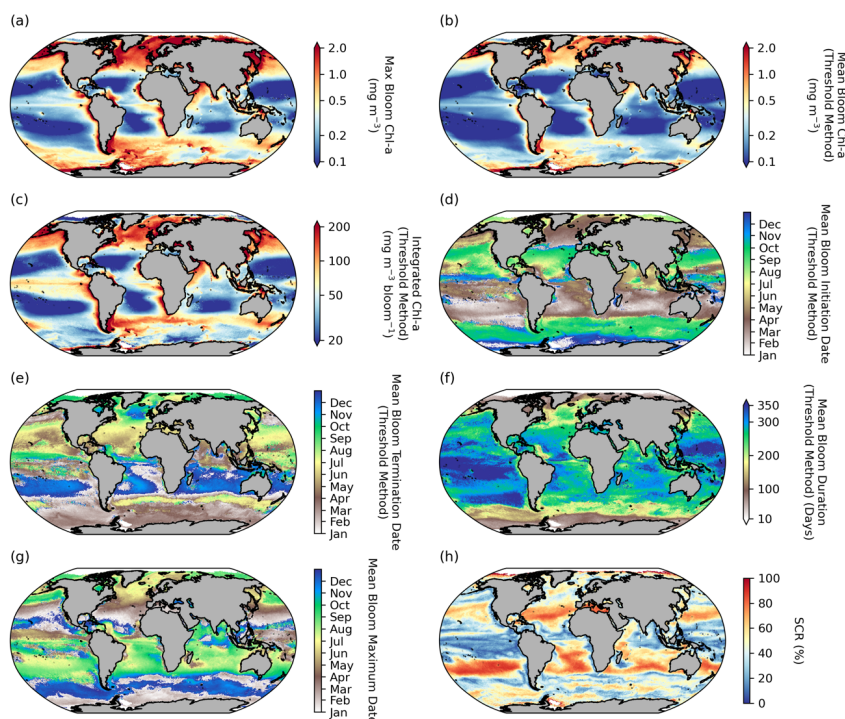


Figure 2: Global distribution of phytoplankton seasonal metrics. Mean [1998 – 2022] maps of (a) bloom max chlorophyll (chl-a), (b) mean chl-a over bloom duration, (c) integrated chl-a over bloom duration, (d) bloom initiation, (e) bloom termination, (f) bloom duration, (g) bloom max chl-a date, and (h) seasonal cycle reproducibility (SCR). Phenological indices (b-f) are determined using the Biomass-based threshold method as defined in Henson et al., 2018; Thomalla et al., 2023.

3.2 Comparison between phenology detection methods

Phytoplankton blooms can initiate rapidly, slowly, be short lived, intermittent, or sustained over a growing season, with different detection methods being more or less sensitive to these varying characteristics of the seasonal bloom (Brody et al., 2013; Ji et al., 2010; Thomalla et al., 2023). In this derived observational data product we have chosen to provide three widely used bloom detection methods for all three resolutions allowing the user to determine which method (or all) is most appropriate for their region and application, (Figure 3 and Figure A2). Indeed, these methods each have their strengths and weaknesses. For example, as explained in Brody et al. (2013), the biomass based TS method will likely capture the bloom start dates at the largest increase in chlorophyll concentrations. It is thus more suitable for studies wanting to investigate the match or mismatch between

- Deleted: of application to
- Deleted: and allow
- Deleted: .
- Formatted: Font colour: Black
- Deleted: , based on
- Deleted: range of bloom amplitude (refer to methods), may be...
- Formatted: Font colour: Black
- Formatted: Font colour: Black
- Formatted: Font colour: Black
- Formatted: Font colour: Black
- Formatted: Font colour: Black, Not Highlight

367 phytoplankton and upper trophic levels as the match-mismatch hypothesis is based on the timing of the high
 368 phytoplankton biomass period (Cushing, 1990). This method has been found to be relatively insensitive to the
 369 percentage of the threshold used (Brody et al., 2013; Siegel et al., 2002). The RC method, which identifies the
 370 bloom initiation as the time when chl-a increases rapidly, is likely more suitable for investigating the physical or
 371 biochemical mechanisms that create conditions in which the bloom occurs (Brody et al., 2013). Whereas the CS
 372 method could be used to identify either of the features above, Brody et al. (2013) showed that, while there are
 373 sensitivities of the CS method to the threshold chosen, the 15% threshold as applied here, is most appropriate at
 374 capturing bloom initiation dates of both subpolar and subtropical regions and thus most appropriate to be applied
 375 across global scales. It is interesting and potentially valuable to determine when and where different methods of
 376 determination agree or disagree, and we advocate for users to apply all three methods so that they may interrogate
 377 the differences and make informed decisions about choosing one over another or utilising all three to define a
 378 range in the desired metric. In Figure 3, the standard deviation (STD) between the three methods is applied
 379 globally to assess the agreement between climatological means from the different methods.

380 Across large regions of the global ocean, there is good agreement between the different methodological
 381 approaches (e.g. the global mean STD for the phenological timing indices is ~8-days) (Figure 3 a- b) All methods
 382 produce similar large-scale patterns (Figure A2 a-c, g-f, m-o). There are however some specific regions where
 383 larger differences in timing emerge of ~30-50 days (Figure 3 and Figure A2 d-f, j-l), which are of a similar order
 384 of magnitude as reported by Brody et al. (2013) who found areas with differences exceeding two months. The
 385 largest differences for both bloom initiation and termination tend to coincide with transitional zones such as at
 386 the boundaries between the subtropical and subpolar gyres in both hemispheres and in all three basins (Figure
 387 3a,b). This is not too surprising, given that these boundaries represent areas of significant biogeochemical
 388 signatures and regime shifts between phytoplankton seasonal characteristics with strong north-south gradients in
 389 bloom metrics (Figure 2). While there are no other comparisons of these detection methods on a global scale, such
 390 differences were similarly seen in Brody et al. (2013) for the North Atlantic bloom, their Figure 4, where the
 391 largest differences between bloom initiation methods occurred at the sharp transition boundaries between the
 392 subtropical and subpolar latitudes. In general, there is stronger agreement between methods in the higher subpolar
 393 latitudes compared to subtropical latitudes, as evidenced by slightly elevated STDs in the subtropical gyres (Figure
 394 3a,b). The subtropical oligotrophic regions are characterised by phytoplankton seasonal cycles that typically have
 395 lower bloom amplitudes, are more gradual and have longer durations (Figure 2). The TS method tends to produce
 396 earlier bloom initiations and earlier terminations in these subtropical regions (Figure A2 d-e, j-k). In these regions
 397 the chl-a min-max range is relatively small, thus a 5% threshold may be exceeded earlier in both termination and
 398 initiation. The RC method, based on the rate of change, is likely to produce later bloom timing dates in more
 399 gradual blooms. There is agreement in the resultant bloom durations between the different methods, with similar
 400 large-scale patterns being reproduced by all three methods (Figure 3c, Figure A2m-o). Unsurprisingly, in the
 401 oligotrophic regions, differences between the methods in bloom duration do not translate to large differences in
 402 the integrated and mean bloom chlorophyll because of the low magnitude of the chlorophyll (Figure 2a-c, Figure
 403 3 c-e). There are however, corresponding regions with more noteworthy disagreements in both duration and mean
 404 and integrated bloom chlorophyll, for example in the energetic regions of the Antarctic Circumpolar Current,

Deleted: (explanation provided in Brody et al., (2013).

Formatted: Font colour: Black

Deleted:).

Deleted: (

Deleted: ,.

Deleted: .

Formatted: Font colour: Auto

Formatted: Font colour: Auto

Deleted: also

Deleted: . The coefficient of variation

Deleted: used here

Deleted: of detection across regional domains (with strong agreement represented by values closest to zero).

Deleted: strong

Deleted: Figure 3). The largest disagreements between

Deleted: detection

Deleted: in bloom termination (Figure 3a), with the most notable differences evident in the boundaries of the southern hemisphere subtropical

Deleted: and of the northern boundary of the subAntarctic zone. With

Deleted: , the largest difference in the detection methods similarly occur in the southern hemisphere notably within the subtropical gyres

Deleted: within the Antarctic Marginal Ice Zone against the Antarctic continent where data is particularly sparse (Figure 3b). Dissonance is also evident

Deleted: transition

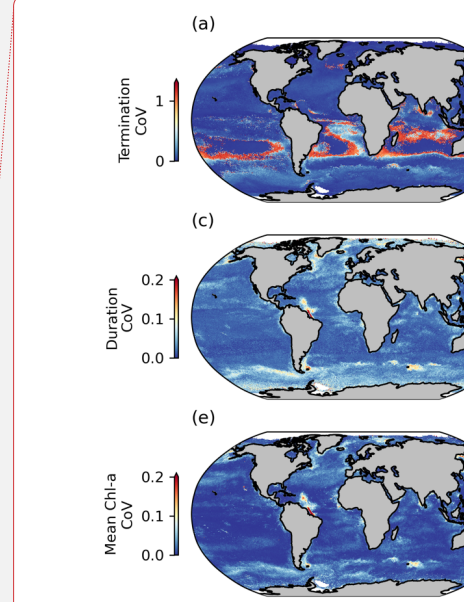
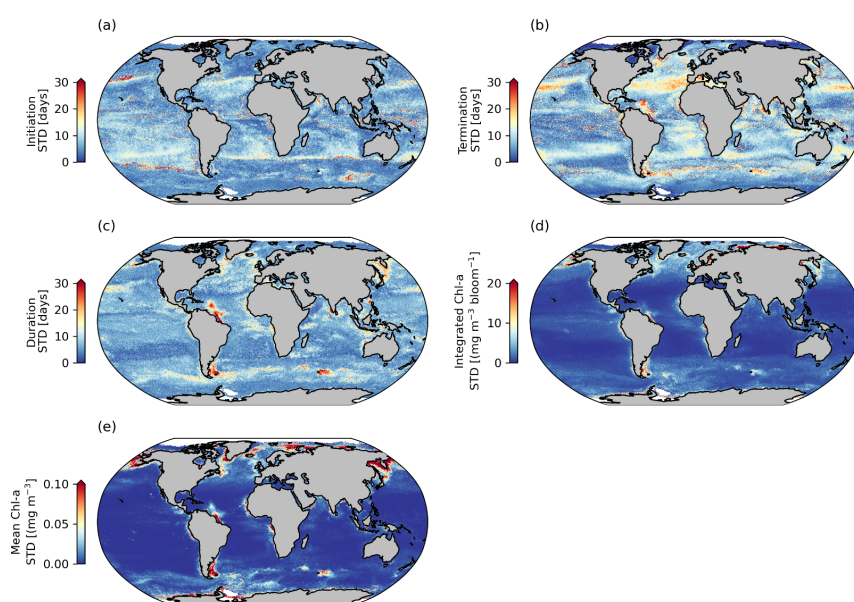
Deleted: Northern Hemisphere.

Deleted: (

Deleted: ,.

Deleted: There is general agreement in bloom duration between the different methods (Figure 3c), with only a ~20-day difference in the climatological global median between TS and the other methods, data not shown. Similarly, for integrated and mean bloom chl-a (Figure 3d, e) there is in general little difference between the methods of detection, with largest differences, as with duration, occurring in the Southern Ocean, particularly around sub-Antarctic Islands, and a localised region of the Atlantic where the Amazon River discharges occurs.

particularly near sub-Antarctic Islands, and localised coastal regions with significant river runoff, such as in the Atlantic where the Amazon River discharge occurs. These areas of large STDs between the methods are driven predominantly by the TS method (Figure A2p-r), which tends to result in shorter blooms, due to later initiations and earlier terminations (Figure A2 d, e, j, k).



Deleted:

Deleted: ,

Deleted: Threshold

Deleted: (TC),

Deleted: Cumulative Sum

Deleted: (CS)

Deleted: Relative Change

Deleted: (RC),

Deleted: b) bloom initiation, (

Deleted: The coefficient of variation (CoV) is calculated as the inter-method standard deviation normalised to the inter-method mean, please note the different scale in panels (a) and (b). ...

Figure 3: Comparisons between phenological detection methods. Shown are standard deviations (STD) calculated between the biomass-based threshold method, the cumulative biomass-based threshold method and the relative of change method, for selected seasonal phytoplankton bloom metrics, including (a) bloom initiation, (b) bloom termination, (c) bloom duration, (d) bloom integrated chl-a and (e) bloom mean chl-a.

3.3. High-resolution phenology indices

The derived phenology data product presented here is offered at three different horizontal resolutions (4, 9 and 25 km), which when compared on a global scale (Figure 4) shows little to no difference in the overall mean distribution of three selected phytoplankton seasonal metrics, including bloom mean chl-a (Figure 4a), bloom duration (Figure 4b) and SCR (Figure 4c). Given that the large-scale distributions of the seasonal metrics remain virtually the same there is little benefit for the user to use the more computationally expensive 4 km product for applications across these larger scales.

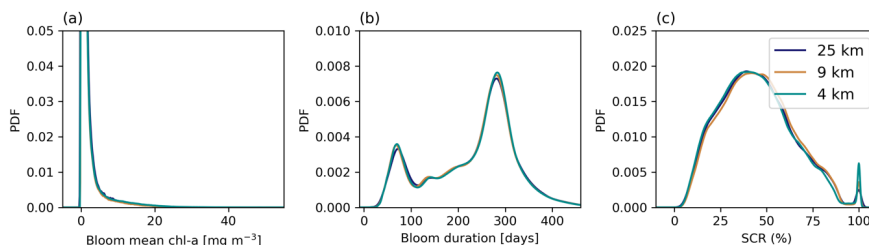


Figure 4: Probability Density Functions (PDF) of climatological mean (calculated from 1998 to 2022) phytoplankton seasonal cycle metrics, compared across three different spatial resolutions (4, 9 and 25 km) for (a) bloom mean chlorophyll-a, (b) bloom duration and (c) seasonal cycle reproducibility (SCR). The TS phenology method is used for (a) and (b).

Deleted: annual

There are, however, notable differences in the resolution of the product on smaller regional scales which appear qualitatively different when compared at two example sites (Figure 5). The sites were selected to reflect regions where a critical dependence is anticipated on the timing and magnitude of seasonal phytoplankton production. The Benguela upwelling system (Figure 5a-c), off the west coast of South Africa is an essential region for supporting key fisheries, while the subAntarctic Kerguelen Island (Figure 5d-f) is a vulnerable marine ecosystem that supports a number of key species. The coarseness of the 25 km product is clearly evident in both sites at these scales, it is considerably more pixelated and there are notable patches where there are differences in the resultant phenological metric between resolutions. For example, in the near-shore of St Helena Bay the integrated bloom chl-a climatology (2017-2022) differs between resolutions from 1654 mg m⁻³ bloom⁻¹, 1841 mg m⁻³ bloom⁻¹, and 1843 mg m⁻³ bloom⁻¹, for the 25 km, 9 km and 4 km maps respectively. At Kerguelen Island, interaction of the Polar Front with shallow bathymetry generates persistent fine-scale ocean dynamics that set strong regional gradients in phytoplankton production (Park et al., 2014). These fine-scale gradients are clearly seen in the spatial variability of bloom duration captured by the higher resolution products. The ‘footprint’ of the island is evident in the extended bloom durations occurring over the shallow plateau associated with the island where there is considerable resuspension of dissolved iron, a key limiting nutrient (Blain et al., 2001). These examples highlight how this data product can be applied to derive valuable indicators for use in national biodiversity assessments, pelagic ecosystems mapping and marine resource management with the added potential of monitoring change in climate sensitive regions relevant for ecosystem services. For regional studies or applications in coastal domains it is recommended that users favour the high spatial resolution product, as it could facilitate detection of finer scale delineations of phenoregions in transitional waters or detect fine scale distributions in phenology metrics that are associated with physical or oceanographic features such as eddies, bays, and upwelling cells. While some phenology indicators produced from daily data could offer additional insights into coastal regions with high temporal variability (e.g., Ferreira et al., 2021), our dataset offers a resource for areas where long gaps in the time-series could negate the use of daily data.

Formatted: Not Superscript/ Subscript

Formatted: Not Superscript/ Subscript

Formatted: Not Superscript/ Subscript

Formatted: Not Superscript/ Subscript

Formatted: Not Superscript/ Subscript

Formatted: Not Superscript/ Subscript

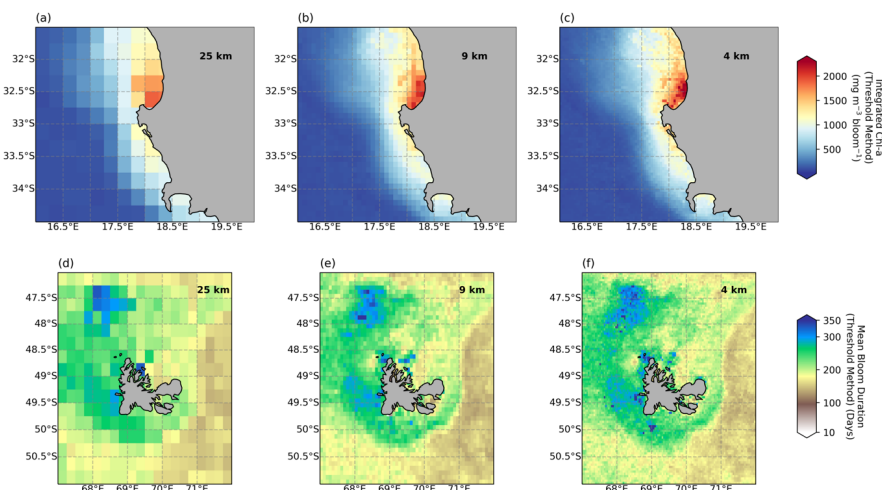


Figure 5: Regional domains comparing the impact of different resolutions (a,d) 25 km, (b,e) 9 km and (c,f) 4 km on (a-c) bloom integrated chl-a and (d-f) the bloom duration averaged from 2017-2022 for (a-c) the Benguela upwelling system off the west coast of South Africa and (d-f) Kerguelen, a subAntarctic island in the Southern Ocean.

4 Data availability

The data are available on the Zenodo repository under the following DOIs, 4 km: 10.5281/zenodo.8402932, 9 km: 10.5281/zenodo.8402847 and 25 km: 10.5281/zenodo.8402823 (Nicholson et al., 2023a, b, c). Chl-a data, used to develop the phytoplankton phenology product, is available from the Ocean Colour–CCI dataset (v.6.0) at <https://esa-oceancolour-cci.org>.

5 Conclusions

The derived observational data product presented here provides a 25-year continuous record of key phytoplankton seasonal cycle metrics (phytoplankton bloom phenology, bloom seasonality and bloom magnitude) on a global-scale. It includes three different phenology detection methods that are widely used by the community. We do not advocate for a particular method over another, the strengths and weaknesses of these different approaches have been highlighted in other studies (e.g., Brody et al., 2013), it is up to the user to choose which (if not all) is the most appropriate for their research applications. The data product is also provided at three different horizontal resolutions (4, 9 and 25 km) for regional versus global-scale application. This product is applicable for a broad range of national to international research and industry applications. Its primary strength is that it can be used to assess, monitor, and understand regional to global-scale characteristics in phytoplankton phenology and to detect

Deleted: Upwelling System

Deleted: Sub-Antarctic

Deleted:).

Formatted: Font colour: Auto

Formatted: Font colour: Auto

Deleted: <https://esa-oceancolour-cci.org>.

Deleted:),

Formatted: Font colour: Auto

change associated with environmental drivers, which is critical for effective management of marine ecosystems and fisheries. This data product will undergo regular updates for future applications and extended time series analysis, which typically happens every two years. It will also be updated when data is temporally extended or when the OC-CCI releases any version updates beyond v.6.0 that will include backwards corrections for previous years, so the entire dataset aligns with the latest version of OC-CCI. This preactive helps to prevent the retention of erroneous values within the data set.

Appendix A

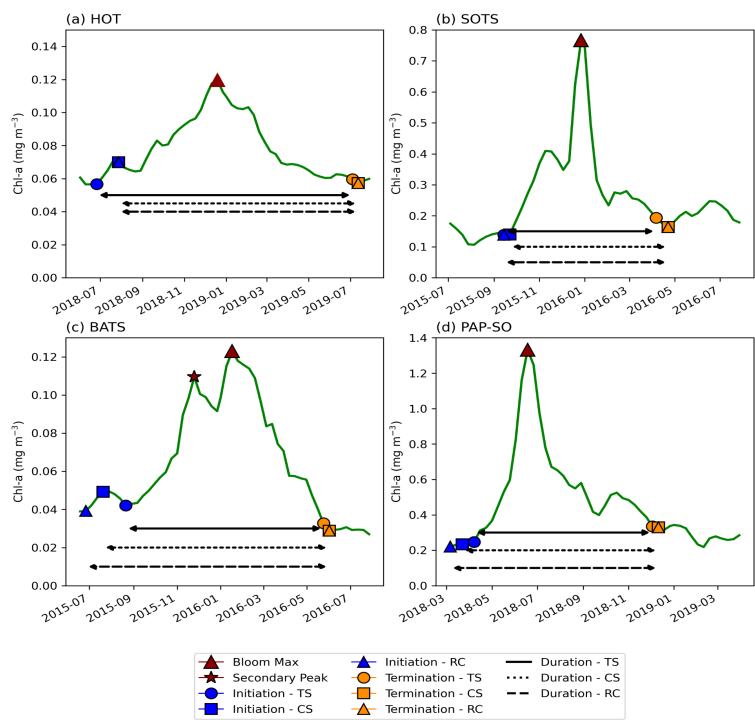


Figure A1: Examples of phytoplankton bloom seasonal cycles and comparisons in phenological detection methods at key sustained observing stations across the global ocean. For (a) Hawaii Ocean Time-series (HOT, 21° 20.6'N, 158° 16.4'W), (b) Southern Ocean Time Series Observatory (SOTS, 140°E, 47°S), (c) Bermuda Atlantic Time-series Study (BATS, 31° 50' N, 64° 10'W) and (d) Porcupine Abyssal Plain (PAP-SO, 49°N, 16.5°W) sustained observatory time-series.

Formatted: Font: Not Bold

Formatted: Not Highlight

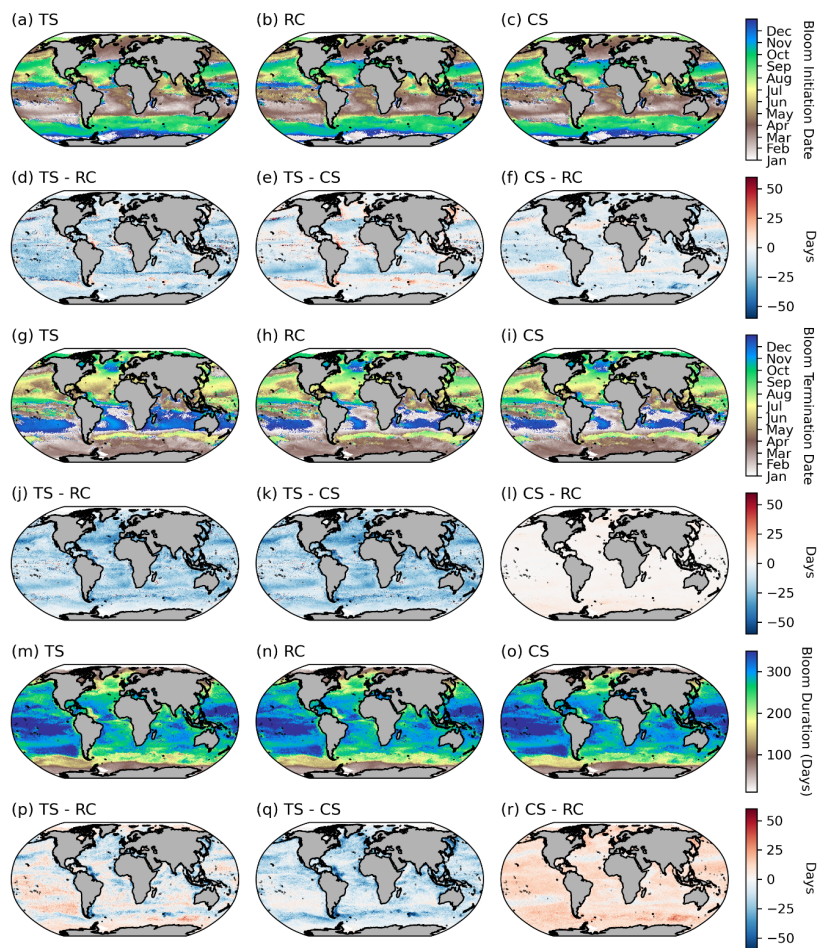


Figure A2. Comparisons between phenological detection methods. The climatological means [1998 - 2022] for (a-c) bloom initiation, (g-i) bloom termination, and (m-o) bloom duration. The differences between the climatological means for the biomass-based threshold method (TS), the cumulative biomass-based threshold method (CS) and the rate of change method (RC) are provided for bloom initiation (d-f), bloom termination (j-l) and bloom duration (p-r).

552 Author contributions. **Conceptualization: SN, TJRK, SJT. Formal analysis: SN, TJRK, MES, Software:**
553 **TRJK, SN, NC. Visualisations: SN, ~~TJRK~~, Writing – original draft: SN. Writing, reviewing, and editing:**
554 **SN, TJRK, SJT, MES, NC.**

Formatted: Font: Bold

Deleted: JRK

Formatted: Font: Bold

555 Competing interests. **The contact author has declared that none of the authors has any competing interests.**

Formatted: Font: Bold

556 Acknowledgements

557 We would like to acknowledge the OC-CCI group for providing the satellite data used in this manuscript. The
558 authors acknowledge their institutional support from the CSIR Parliamentary Grant (0000005278) and the
559 Department of Science and Innovation. We similarly acknowledge the Centre for High-Performance Computing
560 (NICIS-CHPC) for the support and computational hours required for the analysis of this work. SN, TRK, ST and
561 NC acknowledge the National Research Foundation (SANAP200324510487; SANAP200511521175;
562 MCR210429598142).

Formatted: Font colour: Auto, Not Highlight

Formatted: Font colour: Auto, Not Highlight

563 References

564 Anjaneyan, P., Kuttippurath, J., Hareesh Kumar, P. V., Ali, S. M., and Raman, M.: Spatio-temporal changes of
565 winter and spring phytoplankton blooms in Arabian sea during the period 1997–2020, J Environ Manage, 332,
566 <https://doi.org/10.1016/j.jenvman.2023.117435>, 2023.

567 Barnes, D. K. A.: Blue Carbon on Polar and Subpolar Seabeds, in: Carbon Capture, Utilization and
568 Sequestration, edited by: Agarwal, R. K., IntechOpen, Rijeka, Ch. 3, <https://doi.org/10.5772/intechopen.78237>,
569 2018.

570 Bennington, V., McKinley, G. A., Dutkiewicz, S., and Ullman, D.: What does chlorophyll variability tell us
571 about export and air-sea CO₂ flux variability in the North Atlantic?, Global Biogeochem Cycles, 23,
572 <https://doi.org/10.1029/2008GB003241>, 2009.

573 Blain, S., Tréguer, P., Belviso, S., Bucciarelli, E., Denis, M., Desabre, S., Fiala, M., Martin Jézéquel, V., Le
574 Fèvre, J., Mayzaud, P., Marty, J.-C., and Razouls, S.: A biogeochemical study of the island mass effect in the
575 context of the iron hypothesis: Kerguelen Islands, Southern Ocean, Deep Sea Research Part I: Oceanographic
576 Research Papers, 48, 163–187, [https://doi.org/https://doi.org/10.1016/S0967-0637\(00\)00047-9](https://doi.org/https://doi.org/10.1016/S0967-0637(00)00047-9), 2001.

577 Boot, A., von der Heydt, A. S., and Dijkstra, H. A.: Effect of Plankton Composition Shifts in the North Atlantic
578 on Atmospheric pCO₂, Geophys Res Lett, 50, <https://doi.org/10.1029/2022GL100230>, 2023.

579 Brody, S. R., Lozier, M. S., and Dunne, J. P.: A comparison of methods to determine phytoplankton bloom
580 initiation, J Geophys Res Oceans, 118, 2345–2357, <https://doi.org/10.1002/jgrc.20167>, 2013.

581 Buitenhuis, E. T., Hashioka, T., and Quéré, C. Le: Combined constraints on global ocean primary production
582 using observations and models, Global Biogeochem Cycles, 27, 847–858, <https://doi.org/10.1002/gbc.20074>,
583 2013.

Carr, M. E., Friedrichs, M. A. M., Schmeltz, M., Noguchi Aita, M., Antoine, D., Arrigo, K. R., Asanuma, I.,
 Aumont, O., Barber, R., Behrenfeld, M., Bidigare, R., Buitenhuis, E. T., Campbell, J., Ciotti, A., Dierssen, H.,
 Dowell, M., Dunne, J., Esaias, W., Gentili, B., Gregg, W., Groom, S., Hoepffner, N., Ishizaka, J., Kameda, T.,
 Le Quéré, C., Lohrenz, S., Marra, J., Mélin, F., Moore, K., Morel, A., Reddy, T. E., Ryan, J., Scardi, M., Smyth,
 T., Turpie, K., Tilstone, G., Waters, K., and Yamanaka, Y.: A comparison of global estimates of marine primary
 production from ocean color, *Deep Sea Research Part II: Topical Studies in Oceanography*, 53, 741–770,
<https://doi.org/10.1016/J.DSR2.2006.01.028>, 2006.

Charlson, R. J., Lovelock, J. E., and Warren, S. G.: Oceanic phytoplankton, atmospheric sulphur, cloud albedo
 and climate, 1987.

Cushing, D. H.: Plankton Production and Year-class Strength in Fish Populations: an Update of the
 Match/Mismatch Hypothesis, *Adv Mar Biol*, 26, 249–293, [https://doi.org/10.1016/S0065-2881\(08\)60202-3](https://doi.org/10.1016/S0065-2881(08)60202-3),
 1990.

Delgado, A. L., Hernández-Carrasco, I., Combes, V., Font-Muñoz, J., Pratolongo, P. D., and Basterretxea, G.:
 Patterns and Trends in Chlorophyll-a Concentration and Phytoplankton Phenology in the Biogeographical
 Regions of Southwestern Atlantic, *J Geophys Res Oceans*, 128, <https://doi.org/10.1029/2023JC019865>, 2023.

DeVries, T.: The Ocean Carbon Cycle, *Annu Rev Environ Resour*, 47, 317–341,
<https://doi.org/https://doi.org/10.1146/annurev-environ-120920-111307>, 2022.

Falkowski, P. G.: The role of phytoplankton photosynthesis in global biogeochemical cycles*, *Photosynthesis
 Research*, Kluwer Academic Publishers, 235–258 pp., 1994.

Fauchereau, N., Tagliabue, A., Bopp, L., and Monteiro, P. M. S.: The response of phytoplankton biomass to
 transient mixing events in the Southern Ocean, *Geophys Res Lett*, 38, <https://doi.org/10.1029/2011GL048498>,
 2011.

Ferreira, A., Brotas, V., Palma, C., Borges, C., and Brito, A. C.: Assessing phytoplankton bloom phenology in
 upwelling-influenced regions using ocean color remote sensing, *Remote Sens (Basel)*, 13, 1–27,
<https://doi.org/10.3390/rs13040675>, 2021.

Field, C. B., Behrenfeld, M. J., Randerson, J. T., and Falkowski, P.: Primary Production of the Biosphere:
 Integrating Terrestrial and Oceanic Components, *Science (1979)*, 281, 237–240,
<https://doi.org/10.1126/science.281.5374.237>, 1998.

Gittings, J. A., Raitsos, D. E., Kheireddine, M., Racault, M. F., Claustre, H., and Hoteit, I.: Evaluating tropical
 phytoplankton phenology metrics using contemporary tools, *Sci Rep*, 9, <https://doi.org/10.1038/s41598-018-37370-4>, 2019.

Gittings, J. A., Raitsos, D. E., Brewin, R. J. W., and Hoteit, I.: Links between phenology of large phytoplankton
 and fisheries in the northern and central red sea, *Remote Sens (Basel)*, 13, 1–18,
<https://doi.org/10.3390/rs13020231>, 2021.

Harris, C. R., Millman, K. J., van der Walt, S. J., Gommers, R., Virtanen, P., Cournapeau, D., Wieser, E.,
 Taylor, J., Berg, S., Smith, N. J., Kern, R., Picus, M., Hoyer, S., van Kerkwijk, M. H., Brett, M., Haldane, A.,
 del Río, J. F., Wiebe, M., Peterson, P., Gérard-Marchant, P., Sheppard, K., Reddy, T., Weckesser, W., Abbasi,
 H., Gohlke, C., and Oliphant, T. E.: Array programming with NumPy, <https://doi.org/10.1038/s41586-020-2649-2>, 17 September 2020.

643 Henson, S. A., Sanders, R., Madsen, E., Morris, P. J., Le Moigne, F., and Quartly, G. D.: A reduced estimate of
 644 the strength of the ocean's biological carbon pump, *Geophys Res Lett*, 38,
 645 <https://doi.org/https://doi.org/10.1029/2011GL046735>, 2011.
 646
 647 Henson, S. A., Cole, H. S., Hopkins, J., Martin, A. P., and Yool, A.: Detection of climate change-driven trends
 648 in phytoplankton phenology, *Glob Chang Biol*, 24, e101–e111, <https://doi.org/10.1111/gcb.13886>, 2018.
 649
 650 Hopkins, J., Henson, S. A., Painter, S. C., Tyrrell, T., and Poulton, A. J.: Phenological characteristics of global
 651 coccolithophore blooms, *Global Biogeochem Cycles*, 29, 239–253, <https://doi.org/10.1002/2014GB004919>,
 652 2015.
 653
 654 Ji, R., Edwards, M., MacKas, D. L., Runge, J. A., and Thomas, A. C.: Marine plankton phenology and life
 655 history in a changing climate: Current research and future directions, *J Plankton Res*, 32, 1355–1368,
 656 <https://doi.org/10.1093/plankt/fbq062>, 2010.
 657
 658 Kahru, M., Brotas, V., Manzano-Sarabia, M., and Mitchell, B. G.: Are phytoplankton blooms occurring earlier
 659 in the Arctic?, *Glob Chang Biol*, 17, 1733–1739, [https://doi.org/https://doi.org/10.1111/j.1365-](https://doi.org/https://doi.org/10.1111/j.1365-2486.2010.02312.x)
 660 [2486.2010.02312.x](https://doi.org/https://doi.org/10.1111/j.1365-2486.2010.02312.x), 2011.
 661
 662 Koeller, P., Fuentes-Yaco, C., Platt, T., Sathyendranath, S., Richards, A., Ouellet, P., Orr, D., Skúladóttir, U.,
 663 Wieland, K., Savard, L., and Aschan, M.: Basin-Scale Coherence in Phenology of Shrimps and Phytoplankton
 664 in the North Atlantic Ocean, *Science* (1979), 324, 791–793, <https://doi.org/10.1126/science.1170987>, 2009.
 665
 666 Korhonen, H., Carslaw, K. S., Spracklen, D. V., Mann, G. W., and Woodhouse, M. T.: Influence of oceanic
 667 dimethyl sulfide emissions on cloud condensation nuclei concentrations and seasonality over the remote
 668 Southern Hemisphere oceans: A global model study, *Journal of Geophysical Research Atmospheres*, 113,
 669 <https://doi.org/10.1029/2007JD009718>, 2008.
 670
 671 Longhurst, A., Sathyendranath, S., Platt, T., and Caverhill, C.: An estimate of global primary production in the
 672 ocean from satellite radiometer data, *J Plankton Res*, 17, 1245–1271, <https://doi.org/10.1093/plankt/17.6.1245>,
 673 1995.
 674
 675 Lutz, M. J., Caldeira, K., Dunbar, R. B., and Behrenfeld, M. J.: Seasonal rhythms of net primary production and
 676 particulate organic carbon flux to depth describe the efficiency of biological pump in the global ocean, *J*
 677 *Geophys Res Oceans*, 112, <https://doi.org/10.1029/2006JC003706>, 2007.
 678
 679 McCoy, D. T., Burrows, S. M., Wood, R., Grosvenor, D. P., Elliott, S. M., Ma, P. L., Rasch, P. J., and
 680 Hartmann, D. L.: Natural aerosols explain seasonal and spatial patterns of Southern Ocean cloud albedo, *Sci*
 681 *Adv*, 1, <https://doi.org/10.1126/sciadv.1500157>, 2015.
 682
 683 Nicholson, S., Ryan-Keogh, T., Thomalla, S., Chang, N., and Smith, M.: Global Phytoplankton Phenological
 684 Indices - 4km resolution, <https://doi.org/10.5281/zenodo.8402932>, October 2023a.
 685
 686 Nicholson, S., Ryan-Keogh, T., Thomalla, S., Chang, N., and Smith, M.: Global Phytoplankton Phenological
 687 Indices - 9km resolution, <https://doi.org/10.5281/zenodo.8402847>, October 2023b.
 688
 689 Nicholson, S., Ryan-Keogh, T., Thomalla, S., Chang, N., and Smith, M.: Global Phytoplankton Phenological
 690 Indices - 25km resolution, <https://doi.org/10.5281/zenodo.8402823>, October 2023c.
 691

692 Palevsky, H. I. and Quay, P. D.: Influence of biological carbon export on ocean carbon uptake over the annual
693 cycle across the North Pacific Ocean, *Global Biogeochem Cycles*, 31, 81–95,
694 <https://doi.org/10.1002/2016GB005527>, 2017.

695
696 Park, K. T., Yoon, Y. J., Lee, K., Tunved, P., Krejci, R., Ström, J., Jang, E., Kang, H. J., Jang, S., Park, J., Lee,
697 B. Y., Traversi, R., Becagli, S., and Hermansen, O.: Dimethyl Sulfide-Induced Increase in Cloud Condensation
698 Nuclei in the Arctic Atmosphere, *Global Biogeochem Cycles*, 35, <https://doi.org/10.1029/2021GB006969>, 2021.

699
700 Park, Y. H., Durand, I., Kestenare, E., Rougier, G., Zhou, M., D’Ovidio, F., Cotté, C., and Lee, J. H.: Polar
701 Front around the Kerguelen Islands: An up-to-date determination and associated circulation of
702 surface/subsurface waters, *J Geophys Res Oceans*, 119, 6575–6592, <https://doi.org/10.1002/2014JC010061>,
703 2014.

704
705 Platt, T., White, G. N., Zhai, L., Sathyendranath, S., and Roy, S.: The phenology of phytoplankton blooms:
706 Ecosystem indicators from remote sensing, *Ecol Modell*, 220, 3057–3069,
707 <https://doi.org/10.1016/J.ECOLMODEL.2008.11.022>, 2009.

708
709 Racault, M. F., Le Quéré, C., Buitenhuis, E., Sathyendranath, S., and Platt, T.: Phytoplankton phenology in the
710 global ocean, *Ecol Indic*, 14, 152–163, <https://doi.org/10.1016/J.ECOLIND.2011.07.010>, 2012.

711
712 Racault, M. F., Sathyendranath, S., and Platt, T.: Impact of missing data on the estimation of ecological
713 indicators from satellite ocean-colour time-series, *Remote Sens Environ*, 152, 15–28,
714 <https://doi.org/10.1016/j.rse.2014.05.016>, 2014.

715
716 Racault, M. F., Sathyendranath, S., Menon, N., and Platt, T.: Phenological Responses to ENSO in the Global
717 Oceans, <https://doi.org/10.1007/s10712-016-9391-1>, 1 January 2017.

718
719 Rogers, A. D., Frinault, B. A. V., Barnes, D. K. A., Bindoff, N. L., Downie, R., Ducklow, H. W., Friedlaender,
720 A. S., Hart, T., Hill, S. L., Hofmann, E. E., Linse, K., McMahon, C. R., Murphy, E. J., Pakhomov, E. A.,
721 Reygondeau, G., Staniland, I. J., Wolf-Gladrow, D. A., and Wright, R. M.: Antarctic Futures: An Assessment of
722 Climate-Driven Changes in Ecosystem Structure, Function, and Service Provisioning in the Southern Ocean,
723 <https://doi.org/10.1146/annurev-marine-010419>, 2019.

724
725 Rolinski, S., Horn, H., Petzoldt, T., and Paul, L.: Identifying cardinal dates in phytoplankton time series to
726 enable the analysis of long-term trends, *Oecologia*, 153, 997–1008, <https://doi.org/10.1007/s00442-007-0783-2>,
727 2007.

728
729 Sapiiano, M. R. P., Brown, C. W., Schollaert Uz, S., and Vargas, M.: Establishing a global climatology of
730 marine phytoplankton phenological characteristics, *J Geophys Res Oceans*, 117,
731 <https://doi.org/10.1029/2012JC007958>, 2012.

732
733 Sathyendranath, S., Brewin, R. J. W., Brockmann, C., Brotas, V., Calton, B., Chuprin, A., Cipollini, P., Couto,
734 A. B., Dingle, J., Doerffer, R., Donlon, C., Dowell, M., Farman, A., Grant, M., Groom, S., Horseman, A.,
735 Jackson, T., Krasemann, H., Lavender, S., Martinez-Vicente, V., Mazeran, C., Mélin, F., Moore, T. S., Müller,
736 D., Regner, P., Roy, S., Steele, C. J., Steinmetz, F., Swinton, J., Taberner, M., Thompson, A., Valente, A.,
737 Zühlke, M., Brando, V. E., Feng, H., Feldman, G., Franz, B. A., Frouin, R., Gould, R. W., Hooker, S. B., Kahru,
738 M., Kratzer, S., Mitchell, B. G., Muller-Karger, F. E., Sosik, H. M., Voss, K. J., Werdell, J., and Platt, T.: An
739 Ocean-Colour Time Series for Use in Climate Studies: The Experience of the Ocean-Colour Climate Change
740 Initiative (OC-CCI), *Sensors*, 19, <https://doi.org/10.3390/s19194285>, 2019.

741

742 Sathyendranath, S., Jackson, T., Brockmann, C., Brotas, V., Calton, B., Chuprin, A., Clements, O., Cipollini, P.,
 743 Danne, O., Dingle, J., Donlon, C., Grant, M., Groom, S., Krasemann, H., Lavender, S., Mazeran, C., Mélin, F.,
 744 Müller, D., Steinmetz, F., Valente, A., Zühlke, M., Feldman, G., Franz, B., Frouin, R., Werdell, J., and Platt, T.:
 745 ESA Ocean Colour Climate Change Initiative (Ocean_Colour_cci): Version 5.0 Data,
 746 <https://doi.org/10.5285/1dbe7a109c0244aaad713e078fd3059a>, 2021.
 747
 748 Seyboth, E., Groch, K. R., Dalla Rosa, L., Reid, K., Flores, P. A. C., and Secchi, E. R.: Southern Right Whale
 749 (*Eubalaena australis*) Reproductive Success is Influenced by Krill (*Euphausia superba*) Density and Climate, *Sci*
 750 *Rep*, 6, <https://doi.org/10.1038/srep28205>, 2016.
 751
 752 Siegel, D. A., Doney, S. C., and Yoder, J. A.: The North Atlantic Spring Phytoplankton Bloom and Sverdrup's
 753 Critical Depth Hypothesis, *Science* (1979), 296, 730–733, <https://doi.org/10.1126/science.1069174>, 2002.
 754
 755 Silva, E., Counillon, F., Brajard, J., Korosov, A., Pettersson, L. H., Samuelsen, A., and Keenlyside, N.: Twenty-
 756 One Years of Phytoplankton Bloom Phenology in the Barents, Norwegian, and North Seas, *Front Mar Sci*, 8,
 757 <https://doi.org/10.3389/fmars.2021.746327>, 2021.
 758
 759 Stock, C. A., John, J. G., Rykaczewski, R. R., Asch, R. G., Cheung, W. W. L., Dunne, J. P., Friedland, K. D.,
 760 Lam, V. W. Y., Sarmiento, J. L., and Watson, R. A.: Reconciling fisheries catch and ocean productivity, *Proc*
 761 *Natl Acad Sci U S A*, 114, E1441–E1449, <https://doi.org/10.1073/pnas.1610238114>, 2017.
 762
 763 Sverdrup, H. U.: On Conditions for the Vernal Blooming of Phytoplankton,
 764 <https://doi.org/https://doi.org/10.1093/icesjms/18.3.287>, 1953.
 765
 766 Thomalla, S. J., Fauchereau, N., Swart, S., and Monteiro, P. M. S.: Regional scale characteristics of the seasonal
 767 cycle of chlorophyll in the Southern Ocean, *Biogeosciences*, 8, 2849–2866, [https://doi.org/10.5194/bg-8-2849-](https://doi.org/10.5194/bg-8-2849-2011)
 768 2011, 2011.
 769
 770 Thomalla, S. J., Racault, M. F., Swart, S., and Monteiro, P. M. S.: High-resolution view of the spring bloom
 771 initiation and net community production in the Subantarctic Southern Ocean using glider data, *ICES Journal of*
 772 *Marine Science*, 72, 1999–2020, <https://doi.org/10.1093/icesjms/fsv105>, 2015.
 773
 774 Thomalla, S. J., Nicholson, S. A., Ryan-Keogh, T. J., and Smith, M. E.: Widespread changes in Southern Ocean
 775 phytoplankton blooms linked to climate drivers, *Nat Clim Chang*, 13, 975–984, [https://doi.org/10.1038/s41558-](https://doi.org/10.1038/s41558-023-01768-4)
 776 023-01768-4, 2023.
 777
 778 Tweddle, J. F., Gubbins, M., and Scott, B. E.: Should phytoplankton be a key consideration for marine
 779 management?, *Mar Policy*, 97, 1–9, <https://doi.org/10.1016/J.MARPOL.2018.08.026>, 2018.
 780
 781 Virtanen, P., Gommers, R., Oliphant, T. E., Haberland, M., Reddy, T., Cournapeau, D., Burovski, E., Peterson,
 782 P., Weckesser, W., Bright, J., van der Walt, S. J., Brett, M., Wilson, J., Millman, K. J., Mayorov, N., Nelson, A.
 783 R. J., Jones, E., Kern, R., Larson, E., Carey, C. J., Polat, İ., Feng, Y., Moore, E. W., VanderPlas, J., Laxalde, D.,
 784 Perktold, J., Cimrman, R., Henriksen, I., Quintero, E. A., Harris, C. R., Archibald, A. M., Ribeiro, A. H.,
 785 Pedregosa, F., van Mulbregt, P., Vijaykumar, A., Bardelli, A. Pietro, Rothberg, A., Hilboll, A., Kloeckner, A.,
 786 Scopatz, A., Lee, A., Rokem, A., Woods, C. N., Fulton, C., Masson, C., Häggström, C., Fitzgerald, C.,
 787 Nicholson, D. A., Hagen, D. R., Pasechnik, D. V., Olivetti, E., Martin, E., Wieser, E., Silva, F., Lenders, F.,
 788 Wilhelm, F., Young, G., Price, G. A., Ingold, G. L., Allen, G. E., Lee, G. R., Audren, H., Probst, I., Dietrich, J.
 789 P., Silterra, J., Webber, J. T., Slavič, J., Nothman, J., Buchner, J., Kulick, J., Schönberger, J. L., de Miranda
 790 Cardoso, J. V., Reimer, J., Harrington, J., Rodríguez, J. L. C., Nunez-Iglesias, J., Kuczynski, J., Tritz, K.,
 791 Thoma, M., Newville, M., Kümmerer, M., Bolingbroke, M., Tartre, M., Pak, M., Smith, N. J., Nowaczyk, N.,
 792 Shebanov, N., Pavlyk, O., Brodtkorb, P. A., Lee, P., McGibbon, R. T., Feldbauer, R., Lewis, S., Tygier, S.,

793 Sievert, S., Vigna, S., Peterson, S., More, S., Pudlik, T., et al.: SciPy 1.0: fundamental algorithms for scientific
794 computing in Python, Nat Methods, 17, 261–272, <https://doi.org/10.1038/s41592-019-0686-2>, 2020.
795
796 Yamaguchi, R., Rodgers, K. B., Timmermann, A., Stein, K., Schlunegger, S., Bianchi, D., Dunne, J. P., and
797 Slater, R. D.: Trophic level decoupling drives future changes in phytoplankton bloom phenology, Nat Clim
798 Chang, 12, 469–476, <https://doi.org/10.1038/s41558-022-01353-1>, 2022.
799
800 Zhuang, J., dussin, raphael, Huard, D., Bourgault, P., Banihirwe, A., Raynaud, S., Malevich, B., Schupfner, M.,
801 Filipe, Levang, S., Gauthier, C., Jüling, A., Almansi, M., RichardScottOZ, RondeauG, Rasp, S., Smith, T. J.,
802 Stachelek, J., Plough, M., Pierre, Bell, R., Caneill, R., and Li, X.: pangeo-data/xESMF: v0.8.2,
803 <https://doi.org/10.5281/ZENODO.8356796>, 2023.
804
805